# Photoelectron Spectroscopic Study of the Reaction of Li and Na with $NiCo_2O_4$

Andreas Thissen, David Ensling, F. Javier Fernández Madrigal, and Wolfram Jaegermann

*Surface Science Institute, Department of Materials Science, Darmstadt University of Technology, Petersenstrasse 23, 64287 Darmstadt, Germany*

Ricardo Alcántara, Pedro Lavela, and José L. Tirado*

*Laboratorio de Química Inorgánica, Universidad de Córdoba, Edificio C3, planta 1, Campus de Rabanales, 14071 Córdoba, Spain*

*Received May 30, 2005. Revised Manuscript Received July 18, 2005*

The in situ chemical reaction of $NiCo_2O_4$ with Li and Na by physical vapor deposition is studied by using high-resolution X-ray photoelectron spectroscopy. The thermal decomposition of the mixed oxalate precursors at 320 °C allows the formation of $NiCo_2O_4$ as nanosized domains. The small particle size facilitates the reaction with Li and Na. During the first steps of the reaction of $NiCo_2O_4$ with both alkali metals, the reduction of both $Ni^{3+}$ and $Co^{3+}$ to the divalent state is demonstrated by XP spectroscopic data. The mechanism of the first steps of the reaction has been unfolded. A first intercalation reaction of the alkali ions in the spinel host structure occurs. In a second step, sodium oxide or lithium oxide is formed, as well as the monoxides.

## Introduction

In recent years, tin-based compounds,[1,2] antimonides,[3] phosphides,[4] and metal transition oxides[5,6] have been envisaged as candidates to be the negative electrode of a new generation of lithium-ion batteries.[1−10] The study of the electrochemical reaction mechanisms between lithium and some of these alternative materials is quite interesting, particularly taking into account that the resulting products can exhibit finely divided particles. Metallic nanoparticles are being extensively studied because of their multiple applications.[11,12] Moreover, by electrochemical reaction of lithium[5] or sodium[6] with metallic oxides, finely divided metallic particles embedded in a matrix of lithium oxide can be formed according to the following:

$$M_xO_y + 2y(\mathrm{Li, Na}) \rightarrow xM + y(Li_2O, Na_2O) \qquad (1)$$

Lithium oxide (or sodium oxide) is reversibly formed and nanometric particles of transition metals are produced if electrodes are based on transition metal oxides.[5,6,10]

In addition, by reaction of hydrogen with metallic oxides, finely divided metallic particles can be also obtained:[13]

$$Fe_3O_4 + 4\,H_2 \rightarrow 3\,Fe + 4\,H_2O \qquad (2)$$

Both (1) and (2) type reactions are useful for reversible energy storage systems.

The surface properties of $NiCo_2O_4$ as well as the easy preparation of fine particles of this material are interesting for different applications, which spread from electrodes in lithium-ion and sodium-ion batteries[6] to catalysts for oxygen electrocatalysis.[12] Concerning the former application, the electrochemical reactions with lithium and sodium were previously reported:

$$NiCo_2O_4 + 8Li \rightarrow Ni + 2Co + 4Li_2O \qquad (3)$$

$$NiCo_2O_4 + 8Na \rightarrow Ni + 2Co + 4Na_2O \qquad (4)$$

However, the total sodium consumption of the first discharge was lower than the expected value according to reaction 4. Moreover, the poorly crystalline nature of the reaction products and the presence of other products resulting from side-reactions with the electrolyte made difficult a detailed characterization of the mechanism of reactions 3 and 4. On the other hand, the usefulness of photoelectron spectroscopy to study reactions of transition metal oxides with Li and Na has been unequivocally demonstrated in several studies.[14,15] In this way, the aim of this work is to

(1) Courtney, I. A.; Dahn, J. R. *J. Electrochem. Soc.* **1997**, *144*, 2045.
(2) Kepler, K. D.; Vaughey, J. T.; Thackeray, M. M. *Electrochem. Solid State Lett.* **1999**, *2*, A307.
(3) Alcántara, R.; Fernández-Madrigal, F. J.; Lavela, P.; Tirado, J. L.; Jumas, J. C.; Olivier-Fourcade, J. *J. Mater. Chem.* **1999**, *9*, 2517.
(4) Alcántara, R.; Tirado, J. L.; Jumas, J. C.; Monconduit, L.; Olivier-Fourcade, J. *J. Power Sources* **2002**, *109*, 308.
(5) Poizot, P.; Laurelle, S.; Grugeon, S.; Dupont, L.; Tarascon, J. M. *Nature* **2000**, *407*, 496.
(6) Alcántara, R.; Jaraba, M.; Lavela, P.; Tirado, J. L. *Chem. Mater.* **2002**, *14*, 2847.
(7) Tirado, J. L. *Mater. Sci. Eng., R* **2003**, *40*, 103.
(8) Besenhard, J. O.; Yang, J.; Winter, M. *J. Power Sources* **1997**, *68*, 87.
(9) Ohzuku, T.; Ariyoshi, K.; Yamamoto, S.; Makimura, Y. *Chem. Lett.* **2001**, 1270.
(10) Alcántara, R.; Jaraba, M.; Lavela, P.; Tirado, J. L. *J. Solid State Chem.* **2002**, *166*, 330.
(11) Fendler, J. H. *Nanoparticles and Nanostructurated Films*; Wiley-VCH: Weinheim, Germany, 1998.
(12) Baydi, M. E.; Tiwari, S. K.; Singh, R. N.; Rehspringer, J. L.; Chartier, P.; Koenig, J. F.; Poillerat, G. *J. Solid State Chemistry* **1995**, *116*, 157.
(13) Otsuka, K.; Kaburagi, T.; Yamada, C.; Takenaka, S. *J. Power Sources* **2003**, *122*, 111.
(14) Dedryvère, R.; Laurelle, S.; Grugeon, S.; Poizot, P.; Gonbeau, D.; Tarascon, J. M. *Chem. Mater.* **2004**, *16*, 1056.

10.1021/cm051138p CCC: $30.25 
Published on Web 08/30/2005

**Table 1. XPS Results of Sodium Deposition on $Na_xNi_yCo_2O_z$ at Step Numbers 1−8**

| stoichiometries | | | | | oxidation states | | | foreign phases [%] | | | | | | |
|---|---|---|---|---|---|---|---|---|---|---|---|---|---|---|
| *x*(Na) | Ni | Co | O | C | $Co^{2+}/Co^{3+}$ | $Ni^{2+}/Ni^{3+}$ | $Ni^{4+}/Ni^{3+}$ | Na1 | Na2 | C1 | C2 | O1 | O2 | $\Delta E_F$ |
| 0.00 | 1.25 | 1.75 | 3.85 | 0.97 | 1.22 | 0.67 | 0.17 | | | 61.76 | 38.24 | 55.12 | 44.88 | 0.00 |
| 0.57 | 1.19 | 1.81 | 4.30 | 1.02 | 1.34 | 0.77 | 0.21 | 76.79 | 23.21 | 79.36 | 20.64 | 49.90 | 50.10 | 0.06 |
| 1.13 | 1.15 | 1.85 | 4.13 | 1.07 | 1.55 | 0.89 | 0.17 | 53.02 | 50.29 | 72.79 | 27.21 | 48.79 | 51.21 | 0.12 |
| 1.51 | 1.10 | 1.90 | 4.73 | 1.07 | 1.66 | 1.03 | 0.17 | 45.97 | 56.78 | 79.46 | 20.54 | 46.87 | 53.13 | 0.16 |
| 2.03 | 1.09 | 1.91 | 4.34 | 0.92 | 1.76 | 1.04 | 0.18 | 45.35 | 56.47 | 70.66 | 29.34 | 47.64 | 52.36 | 0.18 |
| 3.29 | 1.06 | 1.94 | 5.65 | 1.36 | 2.11 | 1.34 | 0.25 | 36.62 | 65.24 | 80.42 | 19.58 | 55.64 | 44.36 | 0.12 |
| 3.55 | 0.98 | 2.02 | 5.41 | 1.64 | 2.15 | 1.38 | 0.20 | 31.52 | 69.19 | 73.35 | 26.65 | 56.87 | 43.13 | 0.16 |
| 4.14 | 1.10 | 1.90 | 5.54 | 1.64 | 2.16 | 1.41 | 0.31 | 29.89 | 69.52 | 65.24 | 34.76 | 58.47 | 41.53 | 0.09 |

**Table 2. XPS Results of Lithium Deposition on $Li_xNi_yCo_2O_z$**

| stoichiometries | | | | | oxidation states | | | foreign phases [%] | | | | | | |
|---|---|---|---|---|---|---|---|---|---|---|---|---|---|---|
| *x*(Li) | Ni | Co | O | C | $Co^{2+}/Co^{3+}$ | $Ni^{2+}/Ni^{3+}$ | $Ni^{4+}/Ni^{3+}$ | Li1 | Li2 | C1 | C2 | O1 | O2 | $\Delta E_F$ |
| 0.00 | 1.24 | 1.76 | 4.07 | 1.16 | 0.71 | 0.70 | 0.20 | | | 41.38 | 58.62 | 48.09 | 51.91 | 0.00 |
| 0.33 | 1.18 | 1.82 | 3.68 | 0.98 | 0.72 | 0.81 | 0.14 | 65.37 | 34.63 | 79.44 | 20.56 | 58.84 | 41.16 | 0.16 |
| 0.60 | 1.18 | 1.82 | 4.77 | 0.70 | 0.82 | 0.86 | 0.11 | 39.12 | 60.88 | 51.79 | 48.21 | 55.27 | 44.73 | 0.16 |
| 1.08 | 1.19 | 1.81 | 3.97 | 0.90 | 0.83 | 0.97 | 0.08 | 44.30 | 55.70 | 82.27 | 17.73 | 60.37 | 39.63 | 0.22 |
| 1.56 | 1.09 | 1.91 | 4.33 | 1.56 | 1.04 | 1.07 | 0.10 | 29.61 | 70.39 | 52.13 | 47.87 | 57.68 | 42.32 | 0.19 |
| 1.76 | 1.09 | 1.91 | 5.03 | 0.93 | 0.77 | 1.06 | 0.10 | 22.07 | 77.93 | 75.54 | 24.46 | 55.14 | 44.86 | 0.19 |

find the details of the in situ chemical reaction of $NiCo_2O_4$ with Li and Na by physical vapor deposition by using X-ray photoelectron spectroscopy (XPS). These results could be taken as a basis for a better understanding of the possibilities of $NiCo_2O_4$ as an electrode material for advanced lithium-ion and sodium-ion batteries.

## Experimental Section

The spinel-type $NiCo_2O_4$ sample was prepared by thermal decomposition of oxalate precursors at 320 °C during 10 h.[6] Transmission electron microscopy (TEM) observation was carried out with a JEOL 2010 CX apparatus, working at 200 kV.

The XPS experiments have been carried out at room temperature in a multichamber ultrahigh vacuum (UHV) system with a surface analysis system (Phi 5700). The base pressure during the measurements was better than $10^{-9}$ mbar. Al K$\alpha$ radiation ($h\upsilon = 1486.6$ eV) from a monochromatized X-ray source was used for XPS. The reaction of alkali metals in the surface of $NiCo_2O_4$ was followed by XPS. For this purpose Li and Na was evaporated in UHV from standard alkali metal dispensers (SAES getters, Italy), using a working current of 6.5 A, and deposited on the $NiCo_2O_4$ sample.

The spectra are given in a binding energy scale referred to the Fermi level of a sputter-cleaned Ag reference sample. Sample stoichiometry ratios, $S_{i,j}$, have been calculated from the XP spectra using the following equation:[16]

$$S_{i,j} = \frac{C_i}{C_j} = \frac{I_i/\mathrm{ASF}_i}{I_j/\mathrm{ASF}_j} \tag{5}$$

where $C_i$ and $C_j$ are the concentrations, $I_i$ and $I_j$ are the background-corrected intensities of the photoelectron emission lines, and $\mathrm{ASF}_i$ and $\mathrm{ASF}_j$ are the atomic sensitivity factors for photoionization of the *i*th and *j*th elements. Equation 5 is only valid for homogeneous element distributions in the sample, while in the analyzed samples the distribution of the deposited Na is expected to be nonhomogeneous. Thus, it must be stressed that the reported stoichiometries are apparent and not the real surface composition of the sample. Background correction is done using the Tougaard algorithm with a Tougaard parameter of $B = 200$. All spectra have been deconvoluted by fitting Voigt profiles to the spectra. The resulting data is summarized in Table 1 for Na and Table 2 for Li.

## Results and Discussion

The TEM micrograph for the as-prepared $NiCo_2O_4$ powders is shown in Figure 1. The thermal decomposition of the mixed oxalate precursors at 320 °C allows the formation of nanosized domains. The average size of the primary particles was ca. 8 nm and preferred (111) and (110) zone axes were also visible and confirmed by Fourier transform of selected areas. It should be noted that nanosized primary particles of spinel oxides tend to agglomerate and monodisperse particles are not commonly observable. This phenomenon is usually found in the literature.[7,12,23]

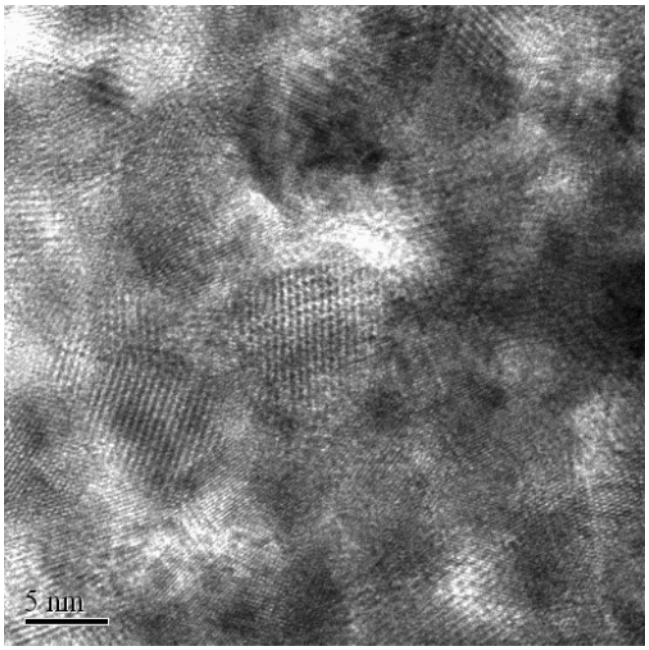


**Figure 1.** HRTEM of exoxalate $NiCo_2O_4$.

(15) Wu, Q. H.; Thissen, A.; Jaegermann, W. *Solid State Ionics* **2004**, *167*, 155.
(16) Wagner, C. D.; Riggs, W. M.; Davis, L. E.; Moulder, J. F. *Handbook of Xray, Photoelectron Spectroscopy*; Perkin-Elmer: Eden Prairie, MN, 1979.
(17) van Veenendaal, M. A.; Sawatzky, G. A. *Phys. Rev. Lett.* **1993**, *70*, 2459.

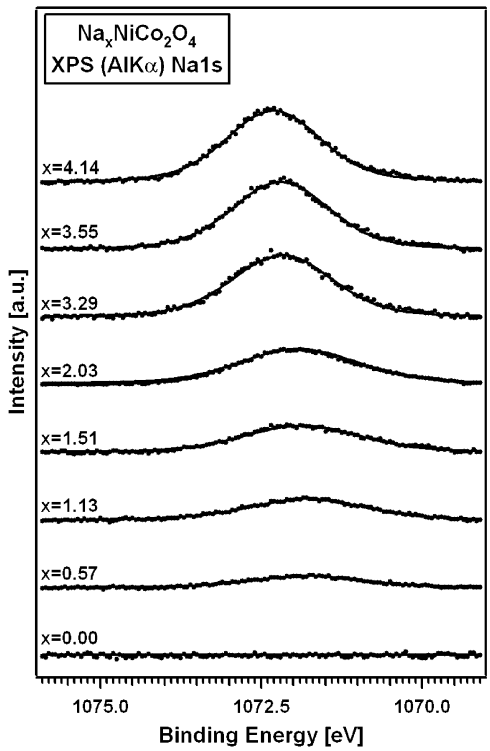


**Figure 2.** XP spectra of the Na1s core level for $NiCo_2O_4$ for different Na concentrations.

XPS is a powerful technique to determine the oxidation state of oxide samples from the analysis of the core level line positions.

**Sodium Deposition.** Recently, several studies on the electrochemical reaction of CoO and $Co_3O_4$ in lithium cells have used XPS as a valuable tool to monitor the changes in the oxidation state of cobalt.[14,26] To our knowledge this is the first report on the change in the oxidation states of Ni and Co in oxides by direct reaction with sodium. The first stages of sodium deposition on $NiCo_2O_4$ can be followed, and the calculated stoichiometries are shown in Table 1 as a function of the deposition step; $x = 0.00$ corresponds to the original spinel sample, while the maximum deposited sodium corresponds to 4.14 Na per $NiCo_2O_4$.

Figure 2 shows the Na1s emission line for different Na exposure times. Sample stoichiometries have been calculated following formula 5 and normalized to $C_{Ni} + C_{Co} = 3$. The $x$ denotes the Na concentration according to this stoichiometry calculation. The maximum value of about $x = 4$ cannot be exceeded by vacuum deposition due to kinetic processes. With increasing Na concentration, the intensity of the Na1s emission increases and is shifted to higher binding energies indicating an upward shift of the Fermi level. The Na1s emission is not very sensitive to chemical shifts. Therefore, in Figure 3 the Na KLL Auger emission is shown, reflecting the general trends already discussed for the Na1s line. Additionally, two components (Na1 and Na2) are visible. Spectral deconvolution (see Table 1) shows that initially Na1 is dominant, while with increasing Na exposure Na2 intensity is increased. In earlier studies[15] it has been shown that Na1 is due to intercalated Na and Na2 originates from oxidized Na. Obviously, the initial process is Na intercalation in the $NiCo_2O_4$ host material. Higher Na concentrations lead then to Na oxide formation. Probably, the ultrafine nature of the spinel oxide particles (see Figure 1) favors the rapid reaction with the incoming sodium atoms and avoids the formation of metallic Na particles. Figures 4 and 5 show the Ni2p and Co2p emission lines. The spectra show a complex profile, containing spin−orbit-doublets and satellites for all oxidation states. The lower energy value is comparable to that of the octahedral $Ni^{2+}$ species found in NiO.[17] Therefore, part of the nickel at the $NiCo_2O_4$ surface is found as $Ni^{2+}$ in octahedral sites. However, the spectra clearly show a higher intensity in the $2p_{3/2}$ profile at higher binding energy, which is in good agreement with the values reported in the literature for $Ni^{3+}$ in $NiCo_2O_4$.[22,23] The intensity ratio for $Ni^{2+}/Ni^{3+}$ lower than unity is consistent with the samples reported produced by thermal decomposition, while sol−gel methods yield higher intensity ratios. Also a small $Ni^{4+}$ component is observed. The full widths at half-maximum, fwhm, of the $2p_{3/2}$ peak components are in the 2−3 eV range. The broadening is ascribable to the fact that each main line is enriched by multiplet structure due to 2p−3d hole−hole interactions and possibly by Ni−Ni intersite interactions known as nonlocal screening. The Co2p XPS region resembles that recorded from $Co_3O_4$[19] and shows components

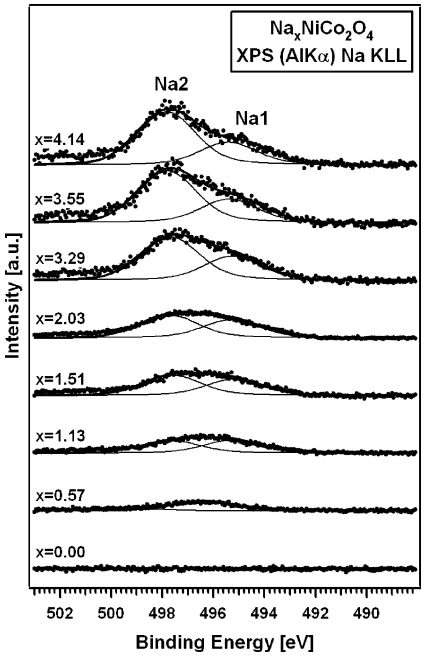


**Figure 3.** Na KLL Auger spectra for $NiCo_2O_4$ for different Na concentrations.

(18) Chuang, T. J.; Brundle, C. R.; Rice, D. W. *Surf. Sci.* **1976**, *59*, 413.
(19) Brundle, C. R.; Chuang, T. J.; Rice, D. W. *Surf. Sci.* **1976**, *60*, 286.
(20) Raquet, B.; Mamy, R.; Ousset, J. C.; Nègre, N.; Goiran, M.; Guerret-Piécourt, C. *J. Magn. Magn. Mater.* **1998**, *184*, 41.
(21) Jiménez, V. M.; Fernández, A.; Espinós, J. P.; González-Elipe, A. R. *J. Electron Spectrosc. Relat. Phenom.* **1995**, *71*, 61.
(22) Marco, J. F.; Gancedo, J. R.; Gracia, M.; Gautier, J. L.; Ríos, E.; Berry, F. J. *J. Solid State Chem.* **2000**, *153*, 74.
(23) Marco, J. F.; Gancedo, J. R.; Gracia, M.; Gautier, J. L.; Ríos, E.; Palmer, H. M.; Greaves, C.; Berry, F. J. *J. Mater. Chem.* **2001**, *11*, 3087.
(24) Roginskaya, Yu. E.; Morozova, O. V.; Lubnin, E. N.; Ulitina, Yu. E.; Lopukhova, G. V.; Trasatti, S. *Langmuir* **1997**, *13*, 4621.
(25) Tavares, A. C.; Cartaxo, M. A. M.; da Silva Pereira, M. I.; Costa, F. M. *J. Electroanal. Chem.* **1999**, *464*, 187.
(26) Fu, Z. W.; Wang, Y.; Zhang, Y.; Qin, Q. Z. *Solid State Ionics* **2004**, *170*, 105.

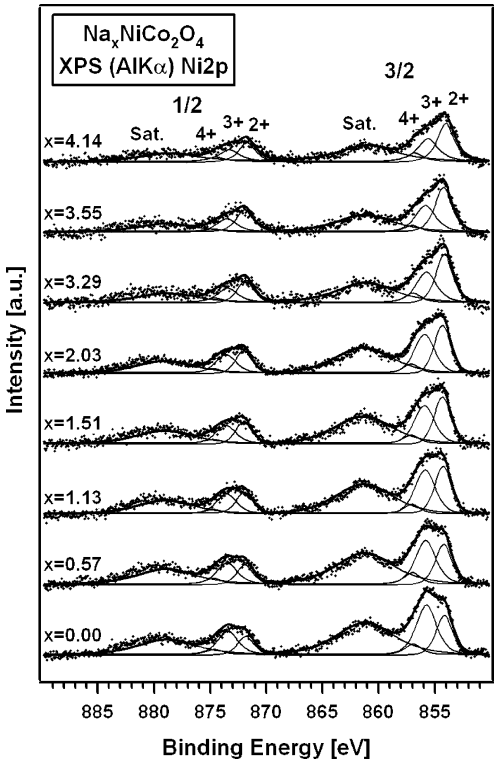


**Figure 4.** Ni2p spectra for $NiCo_2O_4$ for different Na concentrations.

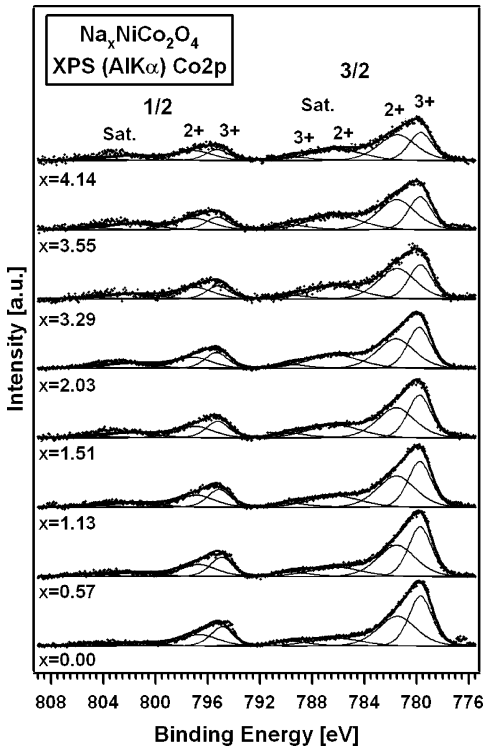


**Figure 5.** Co2p spectra for $NiCo_2O_4$ for different Na deposition steps.

due to $Co^{2+}$ and $Co^{3+}$. The satellite peaks in Figure 4 result from different final states accessible through the band structure of the 3d rocksalt monoxides. Thus, the satellites can be ascribed to a final state of $2p^53d^8$, while the main peak can be assigned to $2p^53d^9L$ where L represents a hole in the 2p level of a neighboring lattice oxide. Deviation from rocksalt stoichiometry in either direction, either by reduction to produce lattice oxygen vacancies or by oxidation, e.g., to form spinel oxides, has been shown to decrease the intensity

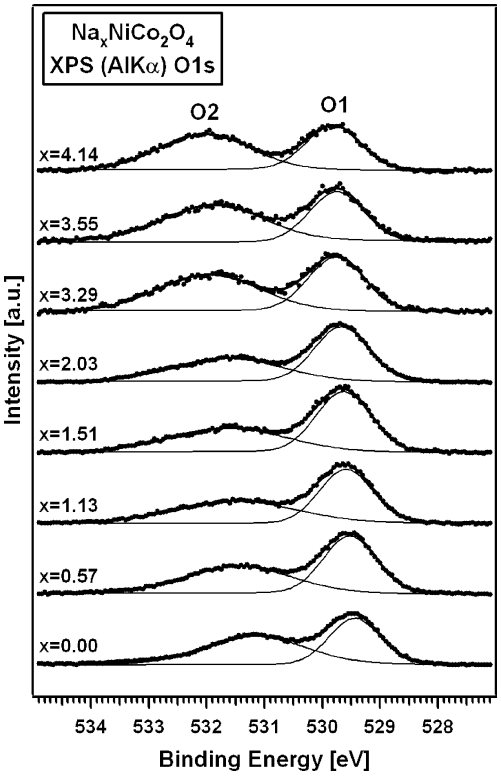


**Figure 6.** XP spectra of the O1s core level for $NiCo_2O_4$ for different Na concentrations.

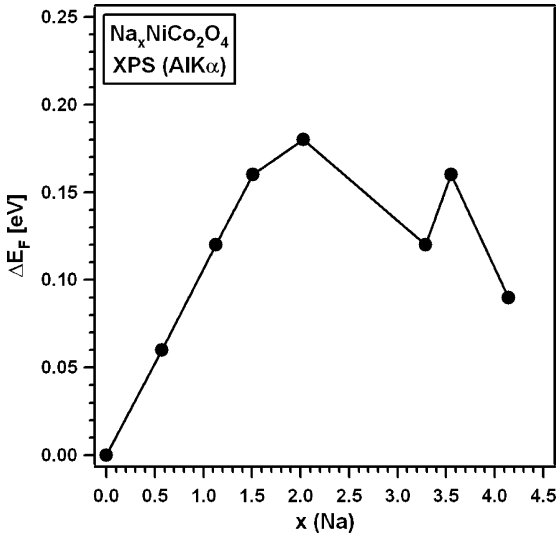


**Figure 7.** Fermi level energy shift vs sodium concentration.

of the satellites dramatically.[27] The observed apparent decrease in the intensity of the satellites in Figure 4, simultaneous to the formation of extra $Ni^{2+}$ ions, can be interpreted if we assume that the newly formed $Ni^{2+}$ oxide deviates from the NiO stoichiometry by the occurrence of oxide vacancies or that the product is a mixed oxide with $Ni_xCo_{1-x}O$ stoichiometry. The Ni/Co atomic ratios for original $NiCo_2O_4$ (Table 1) are slightly higher than the value of 0.5 expected for the stoichiometric compound. This means a slight enrichment in Ni at the surface of the particles. The low intensity of the satellites allows us to discard the presence of CoO impurities. For $Co_3O_4$, Raquet et al.[20] showed that

(27) Nydegger, M. W.; Couderc, G.; Langell, M. A. *Appl. Surf. Sci.* **1999**, *147*, 58.

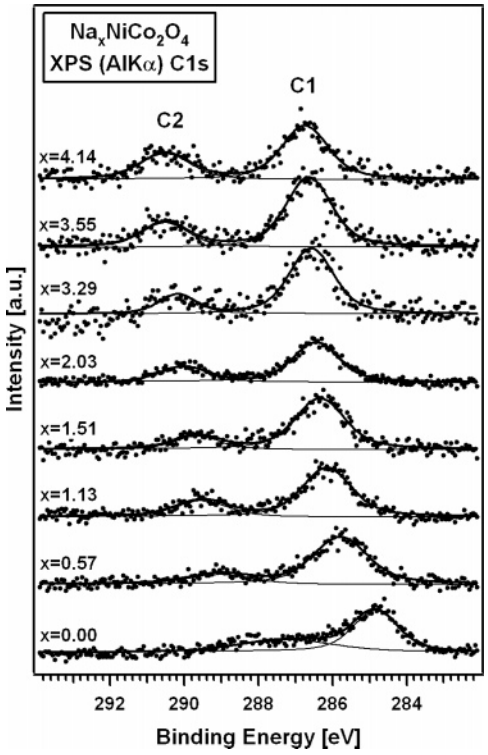


**Figure 8.** C1s spectra for $NiCo_2O_4$ for different Na concentrations.

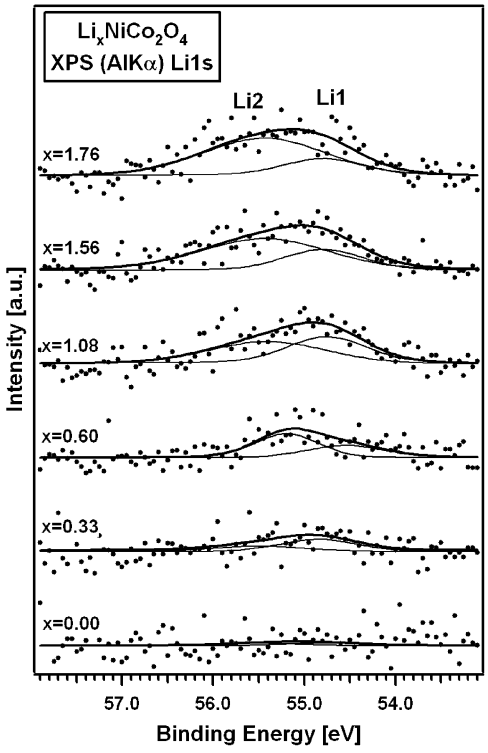


**Figure 9.** Li1s XP spectra as a function of lithium concentration on $NiCo_2O_4$.

the satellite structure (786 eV) of the $Co2p_{3/2}$ peak (780.5 eV) identifies unambiguously CoO, because octahedral $Co^{2+}$ ions presents a strong satellite shake-up structure on the Co2p states, which is interpreted as a result of ligand to metal charge transfer during the photoemission process. Spectra have been deconvoluted following literature results of Marco et al.[22,23] (see Table 1). Obviously, with increasing Na concentration Ni and Co are reduced. The 2+/3+ ratio is

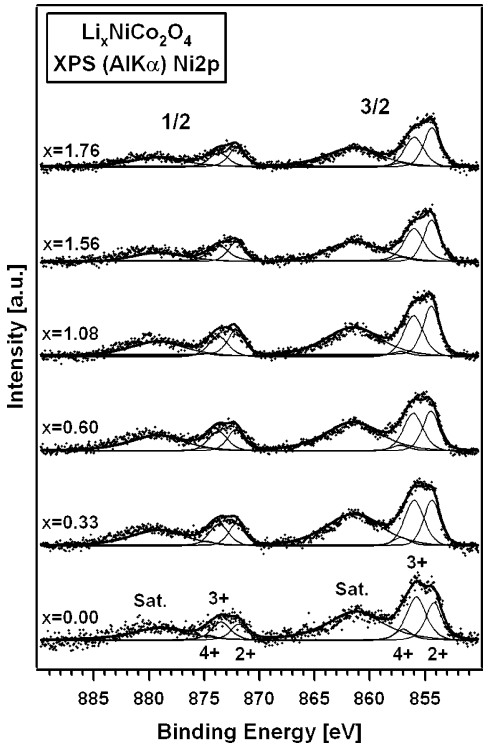


**Figure 10.** $Ni2p_{3/2}$ and $Ni2p_{1/2}$ core levels XP spectra as a function of lithium concentration on $NiCo_2O_4$.

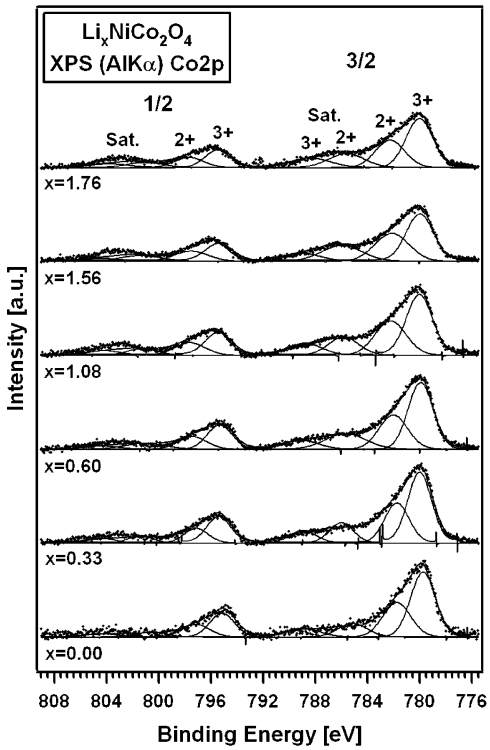


**Figure 11.** Co2p XP spectra as a function of lithium concentration on $NiCo_2O_4$.

increased, and the $Ni^{4+}$ component is significantly weakened. The presence of $Ni^{4+}$ in the mixed oxide after deposition of Na (and Li, Table 2) and the increase in the $Ni^{4+}/Ni^{3+}$ ratio with Na deposition suggest that $Ni^{3+}$ is reduced more easily than $Ni^{4+}$, which in turn has a special stability in octahedral LS $t_{2g}^6$ configuration. Such behavior is similar to that found for $LiNi_{0.5}Mn_{1.5}O_4$ spinel electrodes, in which oxidation−

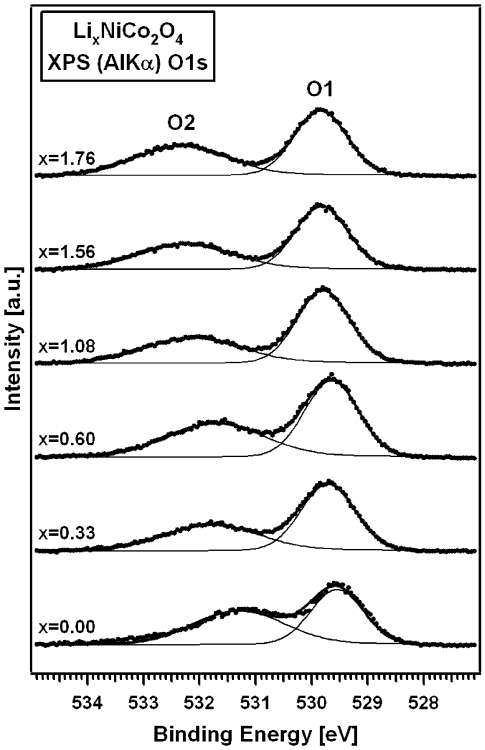


**Figure 12.** O1s XP spectra as a function of lithium concentration on $NiCo_2O_4$.

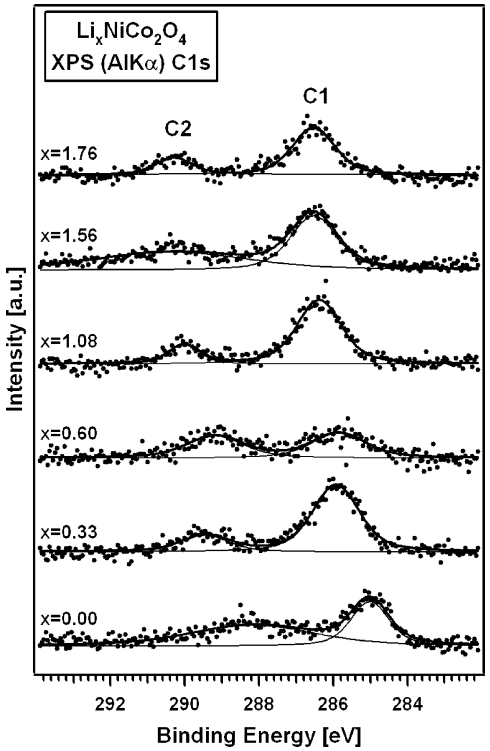


**Figure 13.** C1s XP spectra a function of lithium concentration on $NiCo_2O_4$.

reduction takes place involving basically $Ni^{2+}$ and $Ni^{4+}$ oxidation states.[30,31] Up to $x = 2$ no intensity damping of both signals is observed, indicating that Na is inserted in the sample instead of growing as a film on the surface. Both signals show a shift to higher binding energies also indicating the Fermi level shift due to charge insertion into the sample.[15] The peak positions suffer little changes with sodium content, in contrast with the electrochemical lithiation of $Co_3O_4$.[26] However, the relative intensity of the $Co^{2+}2p_{1/2}$ and $2p_{3/2}$ components increase with sodium content as referred to the same components of $Co^{3+}$. In addition, from the two satellite peaks of $Co2p_{3/2}$ corresponding to $Co^{3+}$ and $Co^{2+}$, which are located at 9.8 eV and at 6.5 eV with respect to the main emission, only the latter increases its intensity on increasing the amount of deposited sodium. Simultaneously, the satellites of $Co2p_{1/2}$ increase their intensity for $Co^{2+}$ when Na deposition is progressing. In contrast with conversion reaction shown in electrochemical lithium cells by other authors,[14,26] no lines at ca. 777.9 eV in the $2p_{3/2}$ region nor at 792.7 eV in the $2p_{1/2}$ region were observed after deposition of ca. 4 sodium atoms per 3 metal atoms. In summary, the XP spectra reveal the reduction of $Co^{3+}$ to $Co^{2+}$ by sodium.

No reduction to the metallic state for Co and Ni and no metallic Na have been observed in these samples. As compared with the pristine spinel sample, the nickel to oxygen and the nickel to cobalt oxygen ratios decrease with the deposition of sodium (Table 1). We can speculate that nickel is first reduced by sodium, and then, metal ion migration results in an enrichment of the surface in cobalt that is needed for the reaction progress.

The O1s emission exhibits two main components (O1 and O2) around 529.5 and 531.2 eV. While the O1 component is, except for the Fermi level shift, unchanged, O2 is shifting away from O1 and is broadened, and its intensity increases with respect to O1. The initial O2 emission is due to hydroxides and carbonates on the surface, while the change with increasing $x$ indicates the sodium oxide formation.[15] Alternative interpretations of these components in cobalt oxides is given by Chuang et al.[18], who studied by XPS the characteristic binding energies in the O1s regions of CoO and $Co_3O_4$. They found that the binding energies of both oxides were identical at $529.50 \pm 0.14$ eV. Then,[19] they ascribed the second O1s component with binding energy in the $531.3 \pm 0.2$ eV range to nonstoichiometric surface oxygen. According to Raquet et al.,[20] the lower energy component is due to Co−O bonds and the other to nonstoichiometry. Jiménez et al.[21] attributed the most intense signal to oxygen atoms in sites with a well-defined coordination, while the other contributions were attributed to low-coordinated oxygen atoms in special sites or domains of the surface where the covalence of the Co−O bond is higher. But in clean and stoichiometric $LiCoO_2$ films, for example, no O2 component is found. Therefore the probability of subsurface oxygen as a reason for O2 is small.

The O1s spectra reported in the literature for $NiCo_2O_4$ materials made by different preparative methods contain four oxygen contributions.[22−25] Apart from the component at 529.9 eV typical of metal−oxygen bonds and the contribution located at the higher binding energy of 531.5 eV associated with oxygen ions in low coordination at the surface, two extra components were deconvoluted.[22] The

(28) Tanaka, S.; Taniguchi, M.; Tanigawa, H. *J. Nucl. Mater.* **2000**, *283−287*, 1405.
(29) Wu, Q. H.; Thissen, A.; Jaegermann, W. *Surf. Sci.* **2005**, *578*, 203.
(30) Zhong, Q. M.; Bonakdarpour, A.; Zhang, M. J.; Gao, Y.; Dahn, J. R. *J. Electrochem. Soc.* **1997**, *144*, 205.
(31) Alcántara, R.; Jaraba, M.; Lavela, P.; Tirado, J. L.; Zhecheva, E.; Stoyanova, R. *Chem. Mater.* **2004**, *16*, 1573.

component at 530.6 eV was ascribed to oxygen in $OH^-$ groups, in agreement with previous literature.[24] Finally, a fourth component was ascribed to a multiplicity of physi- and chemisorbed water on the particles surface. In the spectra of our sample in Figure 6, these two latter components could not be resolved. This is an expected result, as our preparative route is based in a precursor with no hydrogen in its composition. In fact, these components are enhanced in the case of the material made by sol−gel methods.[22] In this work, no further deconvolution of O2 has been performed, because with the limited resolution of O2 no significant information about line positions and fwhm can be derived. Figure 7 shows the changes in the Fermi level position indicating initial intercalation (Fermi level shift up to $x = 1.50$) and the oxide formation (fluctuating values below the maximum Fermi level energy). Finally, the spectra of C1s confirm the presence of adsorbed hydrocarbons (C1) and carbonates (C2) contaminating the surface (Figure 8). The different binding energies between pristine and sodiated spinel reflects the different interactions of the carbonate groups with the particle surface depending on the presence of the basic sodium oxide. Others contaminant were not observed.

From the above results, the mechanism of the first steps of reduction with sodium deposited from the gas phase can be summarized in the following equations:

$$NiCo_2O_4 + x\mathrm{Na} \rightarrow Na_xNiCo_2O_4\ (x \approx 1.0) \qquad (6)$$

$$Na_xNiCo_2O_4 + (2 - x)\mathrm{Na} \rightarrow \mathrm{NiO{\cdot}2CoO} + Na_2O \qquad (7)$$

**Lithium Deposition.** The deposition of Li in the sample is observed as an increase of the XP signal coming from the spectra corresponding to the Li 1s core level (Figure 9). The maximum amount of lithium that can be deposited by the vacuum technique using a commercial dispenser was only about 1.76 Li per formula (Table 2). However, the enhanced peak broadening indicates possible contributions from intercalated and ionic lithium. Deconvolution has been performed using previous results.[28,29] Two components, Li1 and Li2, have been found originating from intercalated (Li1) and oxidized (Li2) lithium. Therefore the process of Li insertion seems to be similar to that of the Na insertion discussed in detail in the previous section. The evolution of the Ni2p (Figure 10), Co2p (Figure 11), O1s (Figure 12), and the amount of carbon contamination (Figure 13) is the same for Li and Na.

Finally, also the Fermi level (Figure 14) tends to increase on increasing the Li deposition (Figure 11) also saturating around $x = 1.00$. However, the sequence is less regular than in the case of the Na-deposited materials (Figure 7). These shifts reflect how intercalation of electron donor species and related charge transfer partially fills up the conduction band of the pristine host. However, not a single insertion process most probably complicates the reactions with lithium, which as a whole may also be written as in the sodium case in equations similar to (6) and (7).

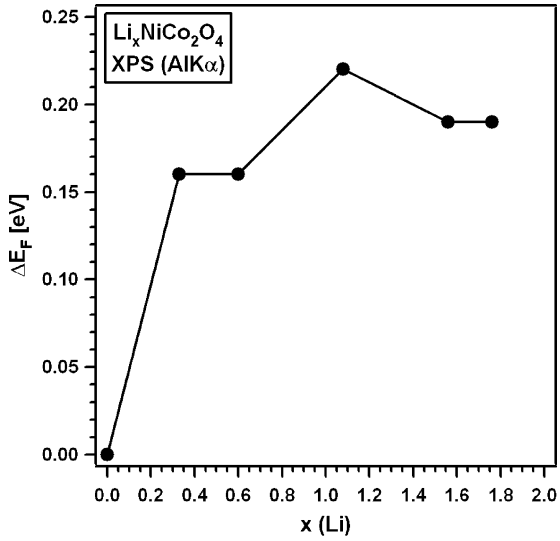


**Figure 14.** Fermi level energy shift vs lithium concentration.

## Conclusions

The small particle size of $NiCo_2O_4$ facilitates the reaction with Li and Na. During the first steps of the reaction of $NiCo_2O_4$ with both alkali metals, the reduction of both $Ni^{3+}$ and $Co^{3+}$ to the divalent state is demonstrated by XP spectroscopic data. The mechanism of the first steps of the reaction has been unfolded. A first intercalation reaction of the alkali ions in the spinel host structure occurs. In a second step, sodium oxide or lithium oxide is formed, as well as the monoxides.

**Acknowledgment.** The authors acknowledge the financial support from MCYT (Contract MAT2002-00434), Acción Integrada hispano-alemana HA02-51, the Deutscher Akademischer Austauschdienst (DAAD), and the Deutsche Forschungsgemeinschaft (DFG). R.A. is indebted to "Programa Ramón y Cajal".

CM051138P